Molecular Cancer Therapeutics

Maytansine and Cellular Metabolites of Antibody-Maytansinoid Conjugates Strongly Suppress Microtubule Dynamics by Binding to Microtubules

Manu Lopus[1], Emin Oroudjev[1], Leslie Wilson[1], Sharon Wilhelm[2], Wayne Widdison[2], Ravi Chari[2], and Mary Ann Jordan[1]

Abstract

Maytansine is a potent microtubule-targeted compound that induces mitotic arrest and kills tumor cells at subnanomolar concentrations. However, its side effects and lack of tumor specificity have prevented successful clinical use. Recently, antibody-conjugated maytansine derivatives have been developed to overcome these drawbacks. Several conjugates show promising early clinical results. We evaluated the effects on microtubule polymerization and dynamic instability of maytansine and two cellular metabolites (*S*-methyl-DM1 and *S*-methyl-DM4) of antibody-maytansinoid conjugates that are potent in cells at picomolar levels and that are active in tumor-bearing mice. Although *S*-methyl-DM1 and *S*-methyl-DM4 inhibited polymerization more weakly than maytansine, at 100 nmol/L they suppressed dynamic instability more strongly than maytansine (by 84% and 73%, respectively, compared with 45% for maytansine). However, unlike maytansine, *S*-methyl-DM1 and *S*-methyl-DM4 induced tubulin aggregates detectable by electron microscopy at concentrations ≥2 μmol/L, with *S*-methyl-DM4 showing more extensive aggregate formation than *S*-methyl-DM1. Both maytansine and *S*-methyl-DM1 bound to tubulin with similar K_D values (0.86 ± 0.2 and 0.93 ± 0.2 μmol/L, respectively). Tritiated *S*-methyl-DM1 bound to 37 high-affinity sites per microtubule (K_D, 0.1 ± 0.05 μmol/L). Thus, *S*-methyl-DM1 binds to high-affinity sites on microtubules 20-fold more strongly than vinblastine. The high-affinity binding is likely at microtubule ends and is responsible for suppression of microtubule dynamic instability. Also, at higher concentrations, *S*-methyl-DM1 showed low-affinity binding either to a larger number of sites on microtubules or to sedimentable tubulin aggregates. Overall, the maytansine derivatives that result from cellular metabolism of the antibody conjugates are themselves potent microtubule poisons, interacting with microtubules as effectively as or more effectively than the parent molecule. *Mol Cancer Ther; 9(10); 2689–99. ©2010 AACR.*

Introduction

Maytansine (Fig. 1) is a 19-member ansa macrolide structure attached to a chlorinated benzene ring (1). It was originally isolated from the shrub *Maytenus ovatus* (2). The antimitotic effect of maytansine has been attributed to its ability to inhibit microtubule assembly by binding to tubulin with a K_D of ~1 μmol/L, at or near the vinblastine-binding site (3–5). Maytansine is effective *in vivo* against Lewis lung carcinoma and B16 murine melanocarcinoma solid tumors and has antileukemic activity against P388 murine lymphocytic leukemia (6). The microtubule-targeted antiproliferative activity of maytansine was substantiated in a screening of 60 human cancer cell types by the U.S. National Cancer Institute (6). Although maytansine inhibits microtubule assembly and kills cancer cells, its utility in the clinic has been hampered by severe side effects and poor efficacy (6). When evaluated as a single agent, maytansine failed to show any significant response in patients with different types of cancers (6, 7).

The recent development of maytansine analogues conjugated to antibodies to increase their target specificity has revived interest in these compounds as potential drugs for cancer chemotherapy (6, 8–10). The present study focuses on the effects of maytansine and its thiomethyl derivatives, *S*-methyl-DM1 and *S*-methyl-DM4 (Fig. 1), which are the primary cellular or liver metabolites of antibody-maytansinoid conjugates prepared with the thiol-containing maytansinoids DM1 and DM4, respectively. Antibody conjugates of DM1 and DM4 kill several

Authors' Affiliations: [1]Department of Molecular, Cellular, and Developmental Biology, and the Neuroscience Research Institute, University of California, Santa Barbara, California and [2]ImmunoGen, Inc., Waltham, Massachusetts

Note: Supplementary material for this article is available at Molecular Cancer Therapeutics Online (http://mct.aacrjournals.org/).

Corresponding Author: Mary Ann Jordan, Department of Molecular, Cellular, and Developmental Biology, and the Neuroscience Research Institute, University of California, Santa Barbara, CA 93106-9610. Phone: 805-893-5317; Fax: 805-893-5081. E-mail: maryann.jordan@lifesci.ucsb.edu

doi: 10.1158/1535-7163.MCT-10-0644

types of cancer cells in the nanomolar to picomolar concentration range (10, 11). Importantly, a recent phase II clinical trial with the maytansinoid conjugate trastuzumab-DM1 has shown promise, yielding an interim overall response rate of 39% in patients with metastatic breast cancer (12). Inside cells, maytansinoid conjugates undergo lysosomal degradation, and the proteolytic digestion of the antibody component of the conjugates gives rise to a number of metabolites (10) that may constitute active drugs. Although the maytansine binding to tubulin and its effects on microtubule assembly have been studied, its effects on microtubule dynamic instability are unknown. In addition, the mechanisms of action of the metabolites of the antibody conjugates, which may ultimately constitute the active intracellular components, are unknown.

Microtubules are dynamic cytoskeletal polymers that switch stochastically between states of growing and shortening, called "dynamic instability" (13). They function in the precise segregation of chromosomes during cell division, transport of cellular cargos, and positioning and movement of intracellular organelles (13, 14). Inhibition of microtubule function leads to cell cycle arrest and cell death (14). Microtubule-targeted drugs, including the *Vinca* alkaloids, taxanes, and epothilones, suppress the dynamic instability of microtubules, induce mitotic arrest, inhibit cell proliferation, and induce apoptosis (15). In this study, we evaluated the effects of maytansine and its two thiomethyl-containing derivatives, *S*-methyl-DM1 and *S*-methyl-DM4, on microtubule dynamic instability, and we determined the binding of *S*-methyl-DM1 to tubulin and microtubules.

Although *S*-methyl-DM1 and *S*-methyl-DM4 inhibited microtubule assembly more weakly than maytansine, they suppressed dynamic instability more strongly than maytansine. As in the case of vinblastine, the maytansinoids potently suppress microtubule dynamic instability by binding to a small number of high-affinity sites, most likely at microtubule ends. Thus, the maytansine derivatives that result from cellular metabolism of the antibody conjugates are themselves potent microtubule poisons, interacting with microtubules as effectively as or more effectively than the parent molecule.

Materials and Methods

Synthesis and chemistry

The thiol-containing maytansinoids DM1 [$N^{2'}$-deacetyl-$N^{2'}$-(3-mercapto-1-oxopropyl)-maytansine] and DM4 [$N^{2'}$-deacetyl-$N^{2'}$-(4-mercapto-4-methyl-1-oxopentyl)-maytansine] were synthesized as previously described (16). Each of these compounds was converted to its respective thiomethyl derivative, *S*-methyl-DM1 [$N^{2'}$-deacetyl-$N^{2'}$-(3-thiomethyl-1-oxopropyl)-maytansine] or *S*-methyl-DM4 [$N^{2'}$-deacetyl-$N^{2'}$-(4-thiomethyl-4-methyl-1-oxopentyl)-maytansine], by reacting them overnight with an excess of methyl iodide and *N*,*N*-diisopropylethylamine in a solution of *N*,*N*-dimethylformamide. The resulting *S*-methylated derivatives, *S*-methyl-DM1 and *S*-methyl-DM4, were purified by reverse-phase preparatory high-performance liquid chromatography eluting with a linear gradient of acetonitrile in deionized water. The purity and identity of each isolated compound were assessed by high-performance liquid chromatography and mass spectroscopy. [^{3}H]DM1 was synthesized as previously described (17) and converted to *S*-[methyl-^{3}H]DM1 by methylation with methyliodide as described for *S*-methyl-DM1 above.

Purification of tubulin and microtubule protein

Bovine brain microtubule protein [MTP; tubulin and microtubule-associated proteins (MAP)] was isolated by two cycles of temperature-dependent polymerization and depolymerization (18). Tubulin was purified from MTP by phosphocellulose chromatography (19) and concentrated to 9 mg/mL in 100 mmol/L PIPES, 1 mmol/L EGTA, and 1 mmol/L $MgSO_4$ (pH 6.8; PEM buffer) at 30°C. Purified tubulin was drop-frozen in liquid nitrogen and stored at −70°C until use. Protein concentration was determined by the method of Bradford using bovine serum albumin as the standard (20).

Effects of the maytansinoids on microtubule polymerization

The ability of maytansine, *S*-methyl-DM1, and *S*-methyl-DM4 to inhibit microtubule assembly was determined by

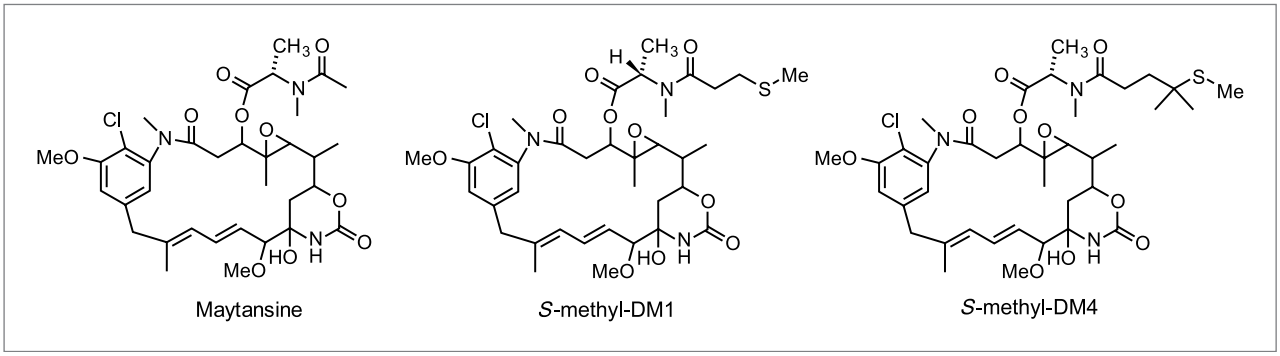

Figure 1. Structures of maytansine and the maytansine thiomethyl analogues *S*-methyl-DM1 and *S*-methyl-DM4.

incubating MTP (3 mg/mL) with a range of maytansinoid concentrations (0–20 μmol/L) in the presence of 1 mmol/L GTP in PEM buffer (30°C, 45 minutes). For sedimentation assays, the polymers formed were centrifuged (35,000 × *g*, 1 hour, 30°C). The microtubule pellets were depolymerized at 0°C overnight and the protein concentrations determined (20). The sedimentation assay for each compound was done at least twice (21). For observing microtubule morphology, samples were fixed in 0.2% glutaraldehyde and stained with 0.5% uranyl acetate (21). The images were acquired at ×50,000 or ×100,000 magnification using a JEOL 1230 transmission electron microscope at 80 kV.

Effects of maytansine and its derivatives on microtubule dynamic instability

Microtubule dynamic instability parameters were measured as previously described (22). Briefly, tubulin (1.5 mg/mL) was assembled on the ends of sea urchin (*Strongylocentrotus purpuratus*) axoneme fragments at 30°C in 87 mmol/L PIPES, 36 mmol/L MES, 1.4 mmol/L $MgCl_2$, 1 mmol/L EGTA (pH 6.8; PMME buffer) containing 2 mmol/L GTP for 30 minutes to achieve steady state. We used a 100 nmol/L concentration of each compound to analyze their individual effects on dynamic instability. Time-lapse images of microtubule plus ends were obtained at 32°C by video-enhanced differential interference contrast microscopy using an Olympus IX71 inverted microscope with a 100× (numerical aperture, 1.4) oil immersion objective. We identified plus ends of the microtubules by their faster growth rate, greater length changes, and larger number of microtubules per axoneme end as compared with the minus ends (22). Microtubule dynamics were recorded for 40 minutes at 30°C, capturing 10 minutes long videos for each area under observation. The rates and durations of growing and shortening and the transition frequencies were determined after tracking the microtubules using RTM-II software (23) and analyzing using IgorPro software (MediaCybernetics). Microtubules were considered as growing if they increased in length by >0.3 μm at a rate of >0.3 μm/min. Shortening events were identified by a >1-μm length reduction at a rate of >2 μm/min. Fifteen to 25 microtubules were analyzed per condition. The catastrophe (a transition from a growing or attenuated state to shortening) frequency was calculated as the total number of catastrophes divided by time spent growing and attenuated (paused). The rescue (transition from shortening to growing) frequency was calculated as the total number of rescue events divided by total time spent shortening. The dynamicity of microtubules was derived as the sum of the total growth length and the total shortening length divided by the total time.

Binding of maytansine or *S*-methyl-DM1 to soluble tubulin

Maytansine or *S*-methyl-DM1 (0–20 μmol/L) was incubated with 3 μmol/L tubulin in PEM buffer for 45 minutes at 30°C. The relative intrinsic fluorescence intensity of tubulin was monitored at 335 nm in a Perkin-Elmer LS 50B spectrofluorometer using a 0.3-cm path length cuvette at an excitation wavelength of 295 nm. The fluorescence emission intensity of *S*-methyl-DM1 and maytansine at this excitation wavelength was negligible. The inner filter effects were corrected using the formula $F_{corrected} = F_{observed} \cdot \text{antilog}\,[(A_{ex} + A_{em})/2]$, where A_{ex} is the absorbance at the excitation wavelength and A_{em} is the absorbance at the emission wavelength. The dissociation constant (K_D) was determined by the following formula: $1/a = K_D/[\text{free ligand}] + 1$, where a is the fractional occupancy of the drug and [free ligand] is the concentration of free maytansine or *S*-methyl-DM1. The fractional occupancy (a) was determined by the formula $a = F/F_{max}$, where F is the change in fluorescence intensity when tubulin and its ligand are in equilibrium and F_{max} is the value of maximum fluorescence change when tubulin is completely bound with its ligand (24). Experiments were done three times.

Stoichiometry of *S*-methyl-DM1 binding to steady-state microtubules

MTP (3 mg/mL) was polymerized to steady state in PEM buffer, and then different concentrations of *S*-[methyl-^{3}H] DM1 (0–4 μmol/L, SA = 145 mCi/mmol) were added at 30°C and incubated for 1 hour. Microtubules were centrifuged at 35,000 × *g* (1 hour, 30°C) through a 0.5-mL glycerol/DMSO cushion (30% glycerol: 10% DMSO). After centrifugation, the supernatant and the cushion were aspirated, and the drug bound to the side of the tubes was carefully removed by overlaying the pellet with 50% glycerol and subsequently aspirating the glycerol from the pellet. The pellets were dissolved in water at 0°C overnight; the protein was measured by Bradford assay; and binding to microtubules was determined after addition to Ready Protein liquid scintillation cocktail (Beckman Coulter) in a Beckman LS1801 scintillation counter. The mean lengths of microtubules in the presence and absence of *S*-methyl-DM1 were determined by electron microscopy (25). Samples were taken at steady state in the presence or absence of *S*-methyl-DM1, fixed in 0.2% glutaraldehyde, and stained with 0.5% uranyl acetate. The images were acquired at ×3,000 magnification using a JEOL 1230 transmission electron microscope at 80 kV for microtubule length measurements (21). From the lengths of microtubules, the amount of the pelleted protein, and the specific activity of *S*-[methyl-^{3}H]DM1, the binding stoichiometry of *S*-methyl-DM1 to microtubules was determined. The K_D for microtubule-*S*-methyl-DM1 interaction was determined as the negative inverse slope of a Scatchard plot of the binding data (26).

Results

Inhibition of microtubule polymerization by maytansine and its thiomethyl analogues

To determine if the thiomethyl analogues of maytansine (the metabolites) retained the basic microtubule-targeted

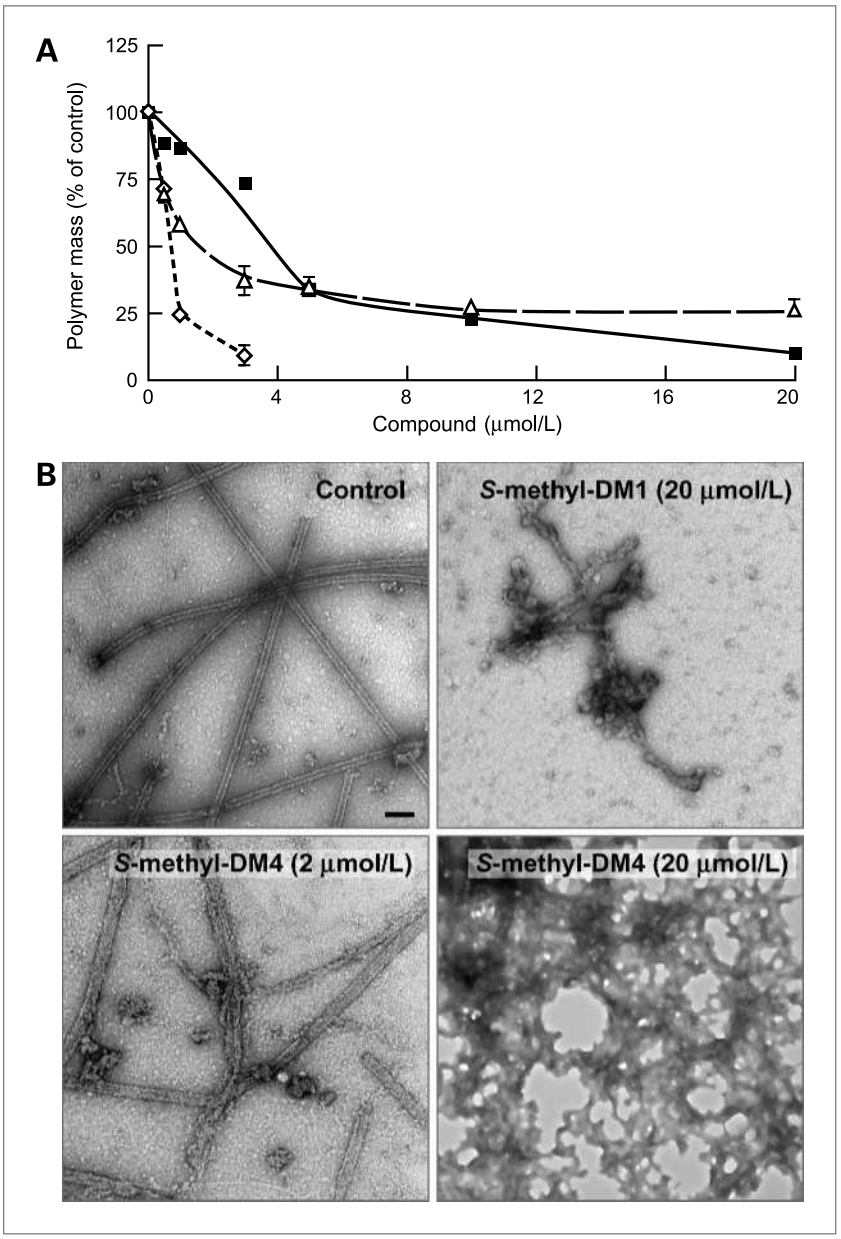

Figure 2. Concentration dependence for inhibition of microtubule assembly by the maytansinoids. A, microtubule protein (3 mg/mL) was assembled in the absence or presence of maytansine (◊), *S*-methyl-DM1 (■), and *S*-methyl-DM4 (△) in the presence of 1 mmol/L GTP in PEM buffer at 30°C for 45 min. The microtubules were collected by centrifugation (35,000 × *g*, 1 h, 30°C) and the amount of sedimented protein was determined. Maytansine, *S*-methyl-DM1, and *S*-methyl-DM4 inhibited microtubule assembly with IC_{50}s of 1 ± 0.02, 4 ± 0.1, and 1.7 ± 0.4 μmol/L, respectively. Points, mean of two experiments; bars, SD. B, electron micrographs of microtubules treated with vehicle (DMSO), *S*-methyl-DM1, or *S*-methyl-DM4. *S*-methyl-DM1 showed few aggregates, whereas *S*-methyl-DM4 induced extensive aggregation. Images are at ×100,000 magnification.

effects of maytansine, we compared the abilities of *S*-methyl-DM1 and *S*-methyl-DM4 to inhibit microtubule polymerization with that of maytansine. Microtubule protein (3 mg/mL) was assembled in the presence or absence of a range of maytansinoid concentrations (0–20 μmol/L, 30°C, 1 hour) and the mass of polymer was determined by sedimentation (Materials and Methods). Under the experimental conditions used, the half-maximal concentration for inhibition of microtubule assembly for maytansine was 1 ± 0.02 μmol/L; for *S*-methyl-DM1, 4 ± 0.1 μmol/L; and for *S*-methyl-DM4, 1.7 ± 0.4 μmol/L (Fig. 2A). Maytansine showed nearly complete inhibition of microtubule polymerization at 3 μmol/L. *S*-methyl-DM1 required a concentration of 20 μmol/L to show a similar effect on polymer mass. *S*-methyl-DM4 did not show complete inhibition of polymer mass. Instead, a plateau at 75% inhibition of polymerization was reached between 10 and 20 μmol/L (Fig. 2A). By electron microscopy, we imaged the polymers formed in the absence or presence of a range of concentrations (0.1, 2, 4, and 20 μmol/L) of maytansine, *S*-methyl-DM1, and *S*-methyl-DM4. At 0.1 μmol/L, the microtubules were intact, with no detectable aggregates, for all three compounds. Maytansine (2 μmol/L) nearly completely inhibited tubulin assembly, showing very few microtubules and no aggregates (images not shown). At higher maytansine concentrations (4 and 20 μmol/L), there were no microtubules or aggregates (images not shown). In contrast, with

S-methyl-DM1 (2 μmol/L), there was a small number of small aggregates along with the microtubules. At 20 μmol/L, *S*-methyl-DM1 showed an increase in aggregate formation. Microtubules predominated, but large aggregates such as those shown in Fig. 2B were also observed frequently. Specifically, we observed two or three of the structures shown in Fig. 2B per 150-mesh grid square. *S*-methyl-DM4 was the most potent inducer of aggregates. At 2 μmol/L *S*-methyl-DM4, we observed aggregates, as well as normal and some imperfect, ragged microtubules with loose protofilamentous structure (Fig. 2B). At 20 μmol/L *S*-methyl-DM4, more extensive aggregation of tubulin occurred with no intact microtubules (Fig. 2B), suggesting that that the plateau observed at higher *S*-methyl-DM4 concentration was due to the formation of aggregates.

Suppression of microtubule dynamic instability by the maytansinoids

We analyzed the effects of maytansine, *S*-methyl-DM1, and *S*-methyl-DM4 on the dynamic instability parameters of individual, reassembled MAP-free bovine brain microtubules at their plus ends at steady state. Microtubule growth and shortening occurred predominantly at the plus ends under the conditions used (Materials and Methods). Life history traces over time showing the changes in length of individual microtubules in the absence and presence of 100 nmol/L maytansinoid are shown in Fig. 3. We used the life history traces to determine the dynamic instability parameters shown in Table 1. Control microtubules displayed typical growth and shortening dynamics (Fig. 3A), whereas incubation with 100 nmol/L maytansine (Fig. 3B), *S*-methyl-DM1 (Fig. 3C), or *S*-methyl-DM4 (Fig. 3D) clearly suppressed dynamic instability. Specifically, all the maytansine analogues suppressed the growing and shortening rates and increased the fraction of time in the attenuated state. The plus ends of control microtubules grew slowly at a mean rate of 1.7 ± 0.2 μm/min, shortened rapidly at a mean rate of 8.9 ± 0.8 μm/min, and occasionally persisted in an attenuated or paused state, neither growing nor shortening detectably (Table 1). Maytansine (100 nmol/L) significantly reduced both the growth and the shortening lengths (by ~40%) and the growth and shortening rates (by 35%). Dynamicity, a measure of the overall addition and loss of tubulin at the microtubule ends per unit time, was suppressed by 45% with 100 nmol/L maytansine.

Interestingly, the thiomethyl maytansinoids were significantly more potent than maytansine in suppressing the dynamic instability of microtubules. For example, *S*-methyl-DM1 showed very strong suppression of dynamic instability, significantly suppressing the shortening rate by 70%, the shortening length by 60%, the catastrophe frequency by 90%, and the dynamicity by 84% (Table 1). This is compared with suppression of the same parameters by maytansine by only 35%, 40%, 30%, and 45%, respectively. The other maytansinoid analogue, *S*-methyl-DM4, affected the dynamic instability parameters in a similar manner as with *S*-methyl-DM1, suppressing the same parameters by 56%, 60%, 90%, and 73%, respectively. Moreover, *S*-methyl-DM1 and *S*-methyl-DM4 increased the percentage of time microtubules remained in a state of attenuated dynamic instability (pause) by 41% and 30%, respectively, whereas maytansine had a negligible effect on the pause state.

Maytansine and *S*-methyl-DM1 bind to soluble tubulin

Using the changes in the intrinsic tryptophan fluorescence of tubulin as a probe for ligand binding, we studied the binding of maytansine and *S*-methyl-DM1 to tubulin. When excited at 295 nm, increasing concentrations of maytansine (0.5–20 μmol/L) or *S*-methyl-DM1 (1–8 μmol/L) showed increasing quenching of tubulin fluorescence, indicating that both maytansinoids

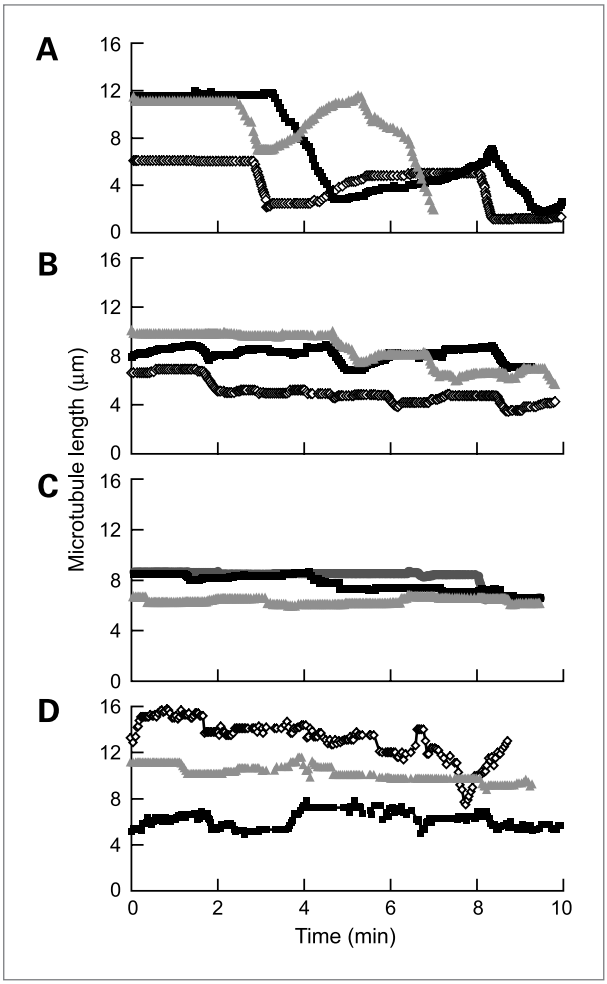

Figure 3. Effect of maytansinoids on microtubule dynamic instability. Life history plots of changes in microtubule length at steady state in the absence and presence of 100 nmol/L compound. A, control; B, maytansine; C, *S*-methyl-DM1; D, *S*-methyl-DM4.

Table 1. Effects of maytansine, *S*-methyl-DM1, and *S*-methyl-DM4 on microtubule dynamic instability

Microtubule dynamic parameters	Control	Maytansine (0.1 μmol/L)	Percent change	*S*-methyl-DM1 (0.1 μmol/L)	Percent change	*S*-methyl-DM4 (0.1 μmol/L)	Percent change
Growth rate (μm/min)	1.7 ± 0.2	1.1 ± 0.2*	35 (–)	1.3 ± 0.4	24 (–)	1.3 ± 0.3	24 (–)
Shortening rate (μm/min)	8.9 ± 0.8	5.8 ± 0.5*	35 (–)	2.7 ± 0.9†	70 (–)	3.9 ± 0.4†	56 (–)
Percent time growing	23.2	24	3.4 (+)	7.3	70 (–)	15.2	34 (–)
Percent time shortening	14.8	11	26 (–)	5.4	64 (–)	4.2	72 (–)
Percent time attenuated	62	65	5 (+)	87.4	41 (+)	80.6	30 (+)
Growing length (μm/event)	1.9 ± 0.2	1.2 ± 0.1†	37 (–)	1 ± 0.1*	47 (–)	1.6 ± 0.1	16 (–)
Shortening length (μm/event)	3 ± 0.2	1.8 ± 0.9†	40 (–)	1.2 ± 0.2‡	60 (–)	1.2 ± 0.2‡	60 (–)
Catastrophe frequency (per minute)	0.30	0.21	30 (–)	0.03	90 (–)	0.03	90 (–)
Rescue frequency (per min)	1.00	0.60	40 (–)	0.56	44 (–)	0.50	50 (–)
Dynamicity	1.3	0.72	45 (–)	0.21	84 (–)	0.35	73 (–)

NOTE: Tubulin was polymerized to steady state with axoneme seeds in the presence of 100 nmol/L maytansinoid and the dynamic instability parameters were determined (Materials and Methods). Fifteen to 25 microtubules were measured for each drug concentration. Data are mean ± SEM.

*$P < 0.05$, versus (Students' *t* test).

†$P < 0.01$, versus control (Students' *t* test).

‡$P < 0.001$, versus control (Students' *t* test).

bind to tubulin (Fig. 4A and B). Analysis of the inverse fractional receptor occupancy of maytansine versus the inverse of the free maytansine concentration gave an equilibrium dissociation constant (K_D) of 0.86 ± 0.23 μmol/L (Fig. 4A). A similar analysis of *S*-methyl-DM1 gave a K_D of 0.93 ± 0.22 μmol/L (Fig. 4B), indicating that both compounds bind relatively strongly to soluble bovine brain tubulin.

S-methyl-DM1 binds to a small number of high-affinity sites at microtubule ends

To gain understanding of the molecular mechanism underlying the suppression of dynamic instability by the maytansinoids, the binding of *S*-methyl-DM1 to steady-state microtubules was investigated using *S*-[methyl-^{3}H]DM1. As described in detail in Materials and Methods, tubulin with MAPs (3 mg/mL) was polymerized to steady state, after which a range of concentrations of radiolabeled *S*-methyl-DM1 were added and incubation was continued for 1 hour. The microtubules and any large sedimentable polymers were collected by centrifugation through a glycerol/DMSO stabilizing cushion. The sedimented protein and the associated radioactivity were determined and the lengths of the microtubules were measured by electron microscopy. Under these conditions, the mean length of the microtubules remained relatively constant (14.4–14.5 μm with a maximum SD of 4 μm at all concentrations between 0 and 100 nmol/L *S*-methyl-DM1, and 13.9–14.1 μm with SD of 4.5 μm at 500 nmol/L–4 μmol/L *S*-methyl-DM1). The mean microtubule lengths were factored into the stoichiometry calculation (drug bound per microtubule) for all concentrations. Under the conditions of the experiment (preassembled MAP-rich microtubules incubated with *S*-methyl-DM1 for only one hour), the microtubule polymer mass decreased by <4% at any of the maytansinoid concentrations. *S*-methyl-DM1 bound to microtubules in a concentration-dependent manner, and the number of maytansinoid molecules bound per microtubule at various concentrations is shown in Fig. 5 and Supplementary Table S1. For example, at 0.1 μmol/L, the concentration of *S*-methyl-DM1 that suppressed dynamicity by 84% (Table 1), 19 ± 1 *S*-methyl-DM1 molecules were bound per microtubule (Fig. 5A). Scatchard analysis (microtubule-bound *S*-methyl-DM1/free *S*-methyl-DM1 versus microtubule-bound *S*-methyl-DM1) indicated that *S*-methyl-DM1 has two types of binding sites on the microtubules or sedimentable aggregates: saturable high-affinity sites and low-affinity sites (Fig. 5B). The equilibrium dissociation constant for *S*-methyl-DM1-microtubule interaction at low drug concentrations (10–100 nmol/L) was 0.1 μmol/L. However, at higher drug concentrations (0.1–4 μmol/L), the binding of *S*-methyl-DM1 to microtubules and sedimentable aggregates that may have been present at higher concentrations showed a second slope that was not saturated even at 4 μmol/L; at this concentration, 210 ± 37 molecules of *S*-methyl-DM1 were bound per microtubule or sedimentable aggregate. Thus, from the *X*-intercept of Fig. 5C and inverse slope, *S*-methyl-DM1 seems to bind to 37 high-affinity sites on microtubules with a K_D of 0.1 ± 0.05 μmol/L and to a large number of low-affinity

sites on microtubules and sedimentable aggregates with a K_D of 2.2 ± 0.2 μmol/L (Fig. 5C).

Discussion

We have examined the molecular mechanisms of action of maytansine and its thiomethyl-containing derivatives, *S*-methyl-DM1 and *S*-methyl-DM4, on purified microtubules *in vitro*. The thiomethyl-containing derivatives were chosen because they represent stable derivatives of the thiol-containing maytansinoids DM1 and DM4 that were used in the preparation of antibody-maytansinoid conjugates and that are currently in clinical evaluation. In addition, these derivatives are the main cellular metabolites of the conjugates and thus may indeed represent the active cytotoxic agents (10).

Inhibition of microtubule assembly by maytansine showed a steep concentration dependence, exhibited the most potent inhibition (IC_{50}, 1 ± 0.02 μmol/L), and induced no formation of aggregates when examined by electron microscopy. In contrast, the two thiomethyl derivatives exhibited shallow concentration-dependent inhibition gradients and somewhat higher IC_{50} values, 1.7 and 4 μmol/L (Fig. 2A), and induced tubulin aggregate formation. *S*-methyl-DM1 induced some small aggregates, particularly at high concentrations (20 μmol/L), whereas *S*-methyl-DM4 induced formation of large, very extensive aggregates (Fig. 2B) at concentrations ≥2 μmol/L, resulting in a plateau in the concentration

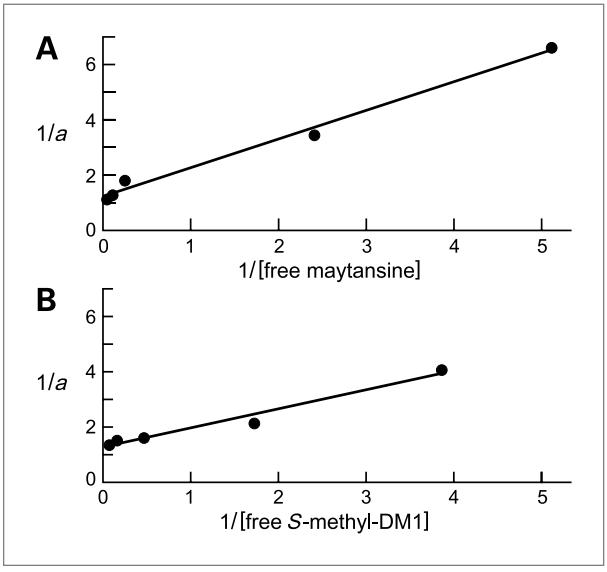

Figure 4. Binding of maytansine (A) or *S*-methyl-DM1 (B) to tubulin. Maytansine (0.5–20 μmol/L) or *S*-methyl-DM1 (1–8 μmol/L) was incubated with 3 μmol/L tubulin in PEM buffer for 45 min at 30°C. The relative intrinsic fluorescence intensity of tubulin was monitored as described in Materials and Methods. The plot indicates a dissociation constant (K_D) of 0.86 ± 0.23 μmol/L for maytansine (A) and 0.93 ± 0.22 μmol/L for *S*-methyl-DM1 (B). The *Y*-axis shows the inverse of the fractional receptor occupancy (*a*) of compound and the *X*-axis shows the inverse of free maytansinoid concentration.

dependence for the quantity of sedimentable polymer at 25% of the control polymer mass between 10 and 20 μmol/L. However, at 100 nmol/L, the concentration at which the effects on dynamic instability were measured, none of the compounds induced detectable tubulin aggregation.

We examined the interactions of maytansine and *S*-methyl-DM1 with soluble tubulin. Maytansine decreased the intrinsic tryptophan fluorescence of tubulin in a concentration-dependent manner. Assuming a single binding site for maytansine on tubulin, linear regression of the data yielded an apparent equilibrium dissociation constant (K_D) of 0.86 ± 0.2 μmol/L (Fig. 4A), similar to the K_D of 0.7 μmol/L reported previously (4). A similar analysis using *S*-methyl-DM1 resulted in a K_D of 0.93 ± 0.2 μmol/L (Fig. 4B), indicating that both maytansine and its derivative bind to soluble tubulin with relatively high affinity.

We also investigated the binding of *S*-methyl-DM1 to microtubules preassembled from purified MAP-rich tubulin. *S*-[methyl-^{3}H]DM1 bound to the microtubules in a concentration-dependent manner (Fig. 5A; Supplementary Table S1). At 100 nmol/L, a concentration that showed strong (84%) suppression of dynamic instability, 19 molecules of *S*-methyl-DM1 were bound per microtubule. At 1 and 4 μmol/L *S*-methyl-DM1, approximately 105 and 210 molecules of *S*-methyl-DM1 were bound per microtubule or to the relatively rare sedimentable aggregates, respectively. Scatchard analysis of the binding of *S*-methyl-DM1 indicated two types of binding sites for this maytansinoid, 37 saturable high-affinity sites per microtubule with an apparent K_D of 0.1 ± 0.05 μmol/L, and several hundred low-affinity sites (Fig. 5B and C) with a 20-fold higher K_D. The affinity of *S*-methyl-DM1 for the 37 high-affinity sites on the microtubule is 9-fold greater than its affinity for soluble tubulin (K_D, 0.9 μmol/L). The low number of very high-affinity binding sites and the strong suppression of dynamic instability events occurring at microtubule ends (catastrophe, rescue, and shortening; Table 1) suggest that *S*-methyl-DM1 potently suppresses dynamic instability through binding to tubulin at the ends of microtubules, which have approximately 13 subunits exposed at each end. The number of high-affinity binding sites is only slightly higher than the number of exposed subunits at the two ends. The reasons for the unusual number of 37 binding sites per microtubule (as compared with 16.8 ± 4.3 high-affinity binding sites for vinblastine and 14.7 ± 1.3 for eribulin; refs. 27, 28) may be due to possible binding at both microtubule ends, slight fraying at microtubule ends resulting in exposure of additional binding sites, or the presence of very small maytansinoid-tubulin oligomers at the microtubule ends (discussed further below).

Suppression of dynamic instability by maytansinoids

Microtubule-targeted agents inhibit cancer cell proliferation by arresting cells at mitosis and inducing them to undergo programmed cell death (15). Many of these

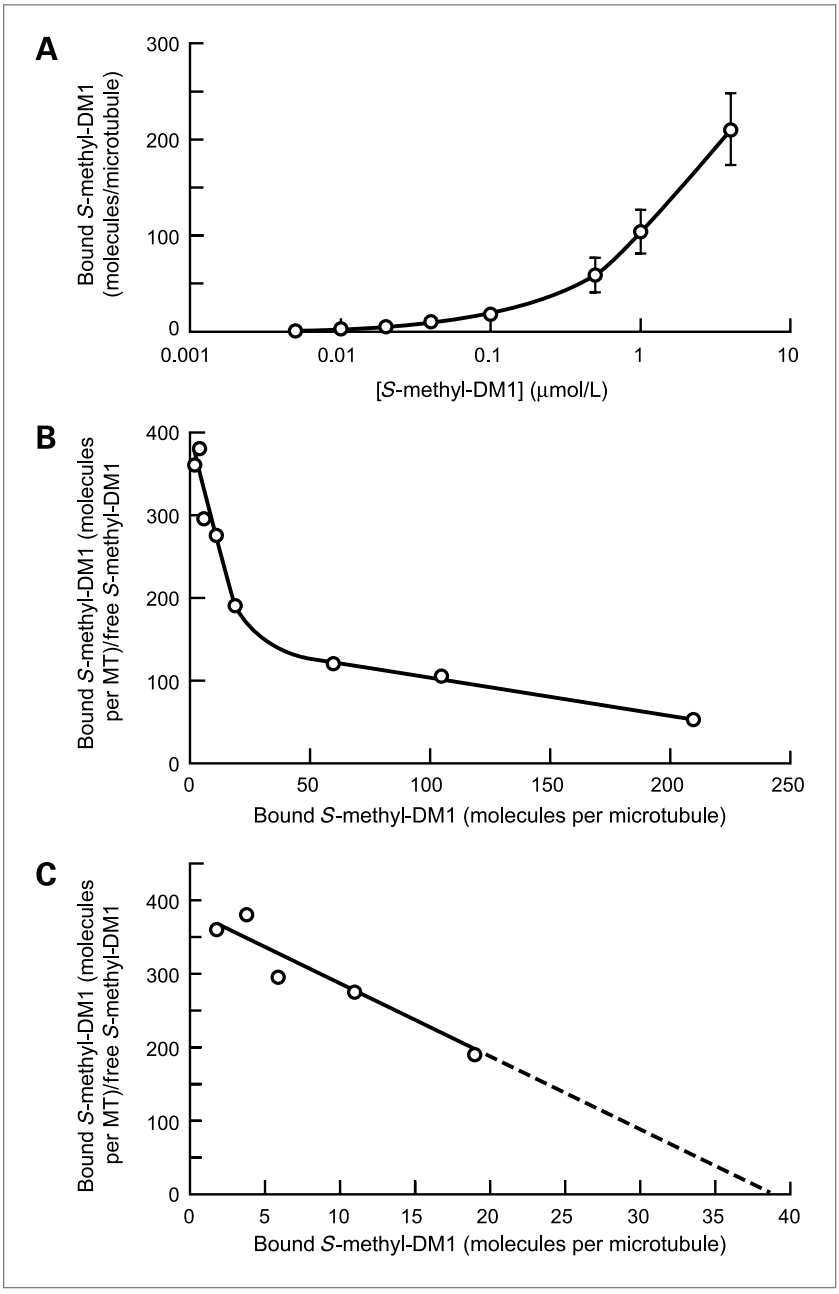

Figure 5. Concentration dependence for binding of *S*-methyl-DM1 to microtubules. A, *S*-methyl-DM1 binds to microtubules in a concentration-dependent manner. Points, mean of three independent experiments; bars, SEM. B, Scatchard plot showing binding to both the high-affinity and low-affinity sites on microtubules. Microtubules were assembled to steady state (MTP, 3 mg/mL) and then incubated with *S*-[methyl-^{3}H]DM1 for 1 h. Microtubules were collected by centrifugation through a glycerol/DMSO cushion. From microtubule lengths, sedimented protein, and incorporated radioactivity, the stoichiometry of the binding of *S*-methyl-DM1 per microtubule was determined. C, Scatchard plot showing binding at low drug concentrations and indicating that there are 37 high-affinity sites at microtubule ends (K_D of 0.1 ± 0.05 μmol/L).

agents do so by suppressing microtubule dynamics at concentrations well below those required to alter microtubule polymer mass (14, 15). We assessed the effects of maytansine, *S*-methyl-DM1, and *S*-methyl-DM4 at a concentration of 100 nmol/L on the dynamic instability of microtubules. At this concentration, *S*-methyl-DM1 and *S*-methyl-DM4 reduced the microtubule polymer mass by less than 3% and maytansine reduced it by 20% (Fig. 2A). A lower concentration of 20 nmol/L *S*-methyl-DM1 was also examined and showed minimal suppression of dynamicity (~6% change; data not shown), indicating that 100 nmol/L was in the appropriate concentration range to assess the effects of the compound on dynamic instability. All three compounds suppressed dynamic instability. Maytansine, as in the case of vinblastine and estramustine (28, 29), suppressed both the growing and the shortening rates to similar extents (35%) and the catastrophe and rescue frequencies similarly (30% and 40%, respectively). In contrast, the thiomethyl derivatives suppressed the rate of shortening more strongly (56–70%) than the rate of growing (~24%), and they suppressed the catastrophe frequency (by 90%) significantly more strongly than the rescue frequency (by only 44–50%). Among the maytansinoids tested, *S*-methyl-DM1 most strongly suppressed the

dynamicity, followed by *S*-methyl-DM4 > maytansine (Table 1). Thus, *S*-methyl-DM1 and *S*-methyl-DM4 both stabilize microtubules more strongly than does maytansine. Although no aggregates were detected at the concentration at which the effects on dynamic instability were measured, it is reasonable to consider that at 100 nmol/L, the maytansine derivatives may have induced formation of very small, undetected aggregates consisting of from two to a few tubulin dimers, either in solution or at the microtubule ends. Such tightly associated drug-tubulin complexes may have effectively capped the microtubule ends, thus inhibiting loss of tubulin from the ends and preferentially inhibiting catastrophe and shortening events and the resultant dynamicity. Thus, they may be responsible for the stronger suppression of microtubule dynamics by *S*-methyl-DM1 and *S*-methyl-DM4 than by maytansine. Aggregated tubulin dimers may also be responsible for the enhanced number of *S*-methyl-DM1 molecules bound to sedimentable polymer at concentrations ≥500 nmol/L (60–210 molecules per microtubule; Supplementary Table S1).

Mechanism of suppression of microtubule dynamic instability by maytansine and its derivatives

Mechanism of suppression of the growth rate. Maytansine and its derivatives suppressed the growth rate of microtubules at 100 nmol/L (Table 1). One possibility is that the suppression of the growth rate is due to a decrease in the association rate constant for tubulin addition. Microtubule growth rate is represented as follows:

$$\mathrm{Rg} = K_{+}C - K_{-} \qquad (1)$$

where the growth rate, Rg, depends on the association rate constant (K_+), the dissociation rate constant (K_-), and the concentration of soluble tubulin (C; ref. 30). As C was not affected by low drug concentrations (100 nmol/L), only a reduction in K_+ or an increase in K_- could contribute to the reduction in the growth rate. Because each of the compounds strongly suppressed the shortening rate also, there was no increase in K_-. Thus, we suggest that a decrease in the association rate constant for tubulin due to the binding of the compound at the tips of microtubules was responsible for the suppression of the growth rate. Moreover, the propensity of maytansine to inhibit GTP exchange of soluble tubulin (31–33) might also have contributed to the decrease in K_+ and thereby suppression of the growth rate.

Mechanism of suppression of the shortening rate, the catastrophe frequency, and the rescue frequency. Maytansine and its derivatives also suppressed the shortening rate (Table 1). The loss of a GTP cap at the tips of the growing microtubules leads to rapid shortening (13). Therefore, suppression of the shortening rate and the catastrophe frequency must occur by a cap-stabilizing mechanism. Maytansine, like vinblastine, does not induce GTP-hydrolysis (31). Maytansine is known as a "pure inhibitor" of microtubule assembly because no alternate polymer structures have been detected (34). Therefore, it is possible that maytansine stabilizes the GTP- (or GDP-Pi) cap because it neither induces detectable alternative lattice structures nor promotes GTP hydrolysis. In addition, the bound drug molecules may stabilize the GTP-bound conformation of tubulin at the microtubule end and thereby inhibit the catastrophe frequency. Maytansine bound at microtubule ends may also stabilize the end against shortening by causing a subtle conformational change in the tubulin at the ends.

The rescue frequency was suppressed by all three maytansinoids to approximately equal extents (40–50%). Maytansine is reported to inhibit the GTP exchange of soluble tubulin (31, 32). The failure to exchange GTP for GDP at the exchangeable nucleotide site on β-tubulin would result in a shortage of GTP-bound tubulin in the reaction mixture. It is reasonable to suggest that the lack of sufficient GTP-bound tubulin inhibits the regain of the stabilizing cap and thus inhibits rescue.

Comparison of the mechanism of actions of maytansinoids and vinblastine

Maytansine is a competitive inhibitor of vincristine binding to tubulin (33). The mechanism of suppression of microtubule dynamics by maytansine and the thiomethyl derivatives has many of the characteristics of the classic end-poisoning mechanism of *Vinca*-domain agents (15), but with some interesting differences. As in the case of vinblastine (35), *S*-methyl-DM1 binds to a few high-affinity sites at the ends of the microtubules. However, unlike vinblastine, where the dissociation constant for the high-affinity binding site is ~1.9 μmol/L (35), the K_D for *S*-methyl-DM1 binding to the small number of high-affinity sites on microtubules is 0.1 μmol/L, indicating that it binds to microtubule ends 19-fold more strongly than vinblastine.

Unlike *Vinca* alkaloids (35), neither maytansine nor its derivatives induced formation of spirals at the ends of the microtubules, as we confirmed by electron microscopy. This observation is consistent with previous evidence indicating that maytansine is a potent inhibitor of tubulin aggregation (5, 34). However, unlike maytansine, *S*-methyl-DM1 and *S*-methyl-DM4 induced formation of irregular small or large aggregates at higher drug concentrations.

Maytansine at a concentration of 100 nmol/L suppressed the growth and shortening rates by 35%, quantitatively similarly to the same concentration of vinblastine (ref. 36; which suppressed the rates by 34% and 47%, respectively). Both compounds suppressed the catastrophe frequency by ~30%. However, in contrast to vinblastine, which enhanced the rescue frequency (~200%), maytansine and its derivatives suppressed the rescue frequency (40–50%). Given that both vinblastine and maytansine share a binding site on tubulin (5) and that both drugs bind at the microtubule tips, their contrasting effects on the rescue frequency are curious. We suggest that these differences may be related, in part, to their different

effects on tubulin-GTP hydrolysis and exchange. Only tubulin dimers with β subunits containing GTP can incorporate into microtubules; continuous replenishment of the β tubulin GTP, by exchanging GDP with GTP, is necessary for microtubule assembly. Roach and Luduena (37) found that maytansine inhibits the formation of a cross-link between Cys12 and Cys 201, a characteristic feature of tubulin depleted of exchangeable nucleotide, significantly more strongly than vinblastine (37). The weak effect of vinblastine on tubulin-GTP exchange can be attributed to its inability to make sufficient contact with the COOH-terminal H6-H7 loop residue Tyr β224 of tubulin (38). In addition, Lin and Hamel (32) found that vinblastine inhibited the rate of GTP hydrolysis twice as strongly as did maytansine. Therefore, we propose that vinblastine promotes attainment of a "GTP-exchange threshold" (due to its significantly weaker inhibition of GTP exchange and its lower rate of GTP hydrolysis), which is responsible for the ability of vinblastine to rescue microtubules from rapid shortening. In contrast, by inhibiting replenishment of β subunit–bound GTP, maytansine may inhibit attainment of the GTP-exchange threshold, thus suppressing rescue.

Disclosure of Potential Conflicts of Interest

The laboratory of the corresponding author (M.A. Jordan) received a gift from ImmunoGen, Inc., in partial support of this work.

Acknowledgments

We thank Herb Miller for preparation of purified microtubules and Victor Goldmacher for helpful suggestions.

Grant Support

NIH grants CA 57291 and NS13560.
The costs of publication of this article were defrayed in part by the payment of page charges. This article must therefore be hereby marked *advertisement* in accordance with 18 U.S.C. Section 1734 solely to indicate this fact.

Received 07/08/2010; accepted 07/26/2010; published 10/11/2010.

References

1. Kupchan SM, Komoda Y, Branfman AR, et al. The maytansinoids. Isolation, structural elucidation, and chemical interrelation of novel ansa macrolides. J Org Chem 1977;42:2349–57.
2. Kupchan SM, Komoda Y, Court WA, et al. Maytansine, a novel antileukemic ansa macrolide from *Maytenus ovatus*. J Am Chem Soc 1972;94:1354–6.
3. Remillard S, Rebhun LI, Howie GA, Kupchan SM. Antimitotic activity of the potent tumor inhibitor maytansine. Science 1975;189:1002–5.
4. Mandelbaum-Shavit F, Wolpert-DeFilippes MK, Johns DG. Binding of maytansine to rat brain tubulin. Biochem Biophys Res Commun 1976;72:47–54.
5. Bhattacharyya B, Wolff J. Maytansine binding to the vinblastine sites of tubulin. FEBS Lett 1977;75:159–62.
6. Cassady JM, Chan KK, Floss HG, Leistner E. Recent developments in the maytansinoid antitumor agents. Chem Pharm Bull (Tokyo) 2004;52:1–26.
7. Annual Report to the FDA by DCT, NCI, on Maytansine, NSC 153858, IND 11857, February 1984.
8. Helft PR, Schilsky RL, Hoke FJ, et al. A phase I study of cantuzumab mertansine administered as a single intravenous infusion once weekly in patients with advanced solid tumors. Clin Cancer Res 2004;10:4363–8.
9. Smith SV. Technology evaluation: cantuzumab mertansine, ImmunoGen. Curr Opin Mol Ther 2004;6:666–74.
10. Erickson HK, Widdison WC, Mayo MF, et al. Tumor delivery and *in vivo* processing of disulfide-linked and thioether-linked antibody-maytansinoid conjugates. Bioconjug Chem 2010;21:84–92.
11. Kovtun YV, Audette CA, Ye Y, et al. Antibody-drug conjugates designed to eradicate tumors with homogeneous and heterogeneous expression of the target antigen. Cancer Res 2006;66:3214–21.
12. Krop I, LoRusso P, Miller KD, et al. A phase II study of trastuzumab-DM1 (T-DM1), a novel HER2 antibody-drug conjugate, in patients with HER2+ metastatic breast cancer who were previously treated with an anthracycline, a taxane, capecitabine, lapatinib, and trastuzumab; San Antonio Breast Cancer Symposium 2009; abstract #710.
13. Lopus M, Yenjerla M, Wilson L. Microtubule dynamics. In: Begley TP, editor. Encyclopedia of chemical biology. 3. New Jersey: John Wiley & Sons; 2009, p. 153–60.
14. Jordan MA, Wilson L. Microtubules as a target for anticancer drugs. Nat Rev Cancer 2004;4:253–65.
15. Jordan MA, Kamath K. How do microtubule-targeted drugs work? An overview. Curr Cancer Drug Targets 2007;7:730–42.
16. Widdison W, Wilhelm S, Cavanagh E, et al. Semisynthetic maytansine analogs for targeted treatment of cancer. J Med Chem 2006;49:4392–408.
17. Xie H, Audette C, Hoffee M, et al. Pharmacokinetics and biodistribution of the antitumor immunoconjugate, cantuzumab mertansine (huC242-1) and its two components in mice. J Pharm Exp Ther 2004;308:1073–82.
18. Farrell KW, Wilson L. Tubulin-colchicine complexes differentially poison opposite microtubule ends. Biochemistry 1984;23:3741–8.
19. Miller HP, Wilson L. Preparation of microtubule protein and purified tubulin from bovine brain by cycles of assembly and disassembly and phosphocellulose chromatography. Methods Cell Biol 2010;95:3–15.
20. Bradford MM. A rapid and sensitive method for the quantitation of microgram quantities of proteins utilizing the principle of protein-dye binding. Anal Biochem 1976;72:248–54.
21. Yenjerla M, Lapointe NE, Lopus M, et al. The neuroprotective peptide NAP does not directly affect polymerization or dynamics of reconstituted neural microtubules. J Alzheimers Dis 2010;19:1377–86.
22. Yenjerla M, Lopus M, Wilson L. Analysis of dynamic instability of steady-state microtubules *In Vitro* by video-enhanced differential interference contrast microscopy. Methods Cell Biol 2010;95:189–202.
23. Walker RA, O'Brien ET, Pryer NK, et al. Dynamic instability of individual microtubules analyzed by video light microscopy: rate constants and transition frequencies. J Cell Biol 1998;107:1437–48.
24. Aneja R, Vangapandu SN, Lopus M, Panda D, Chandra R, Joshi HC. Development of a novel nitro-derivative of noscapine for the potential treatment of drug-resistant ovarian cancer and T-cell lymphoma. Mol Pharmacol 2006;69:1801–9.
25. Jordan MA, Ojima I, Rosas F, et al. Effects of novel taxanes SB-T-1213 and IDN5109 on tubulin polymerization and mitosis. Chem Biol 2002;9:93–101.
26. Rosenthal HE. A graphic method for the determination and presentation of binding parameters in a complex system. Anal Biochem 1967;20:525–32.
27. Smith JA, Wilson L, Azarenko O, et al. Eribulin binds at microtubule ends to a single site on tubulin to suppress dynamic instability. Biochemistry 2010;49:1331–7.

28. Wilson L, Jordan MA, Morse A, Margolis RL. Interaction of vinblastine with steady state microtubules *in vitro*. J Mol Biol 1982;159:125–49.
29. Jordan MA, Walker D, de Arruda M, Barlozzari T, Panda D. Suppression of microtubule dynamics by binding of cemadotin to tubulin: possible mechanism for its antitumor action. Biochemistry 1998;37: 17571–8.
30. Panda D, Daijo JE, Jordan MA, Wilson L. Kinetic stabilization of microtubule dynamics at steady state *in vitro* by substoichiometric concentrations of tubulin-colchicine complex. Biochemistry 1995;34:9921–9.
31. Correia JJ. Effects of antimitotic agents on tubulin-nucleotide interactions. Pharmacol Ther 1991;52:127–47.
32. Lin CM, Hamel E. Effects of inhibitors of tubulin polymerization on GTP hydrolysis. J Biol Chem 1981;256:9242–5.
33. York J, Wolpert-DeFilippes MK, Johns DG, Sethi VS. Binding of maytansinoids to tubulin. Biochem Pharmacol 1981;30:3239–43.
34. Fellous A, Ludueña RF, Prasad V, et al. Effects of Tau and MAP2 on the interaction of maytansine with tubulin: inhibitory effect of maytansine on vinblastine-induced aggregation of tubulin. Cancer Res 1985; 45:5004–10.
35. Singer WD, Jordan MA, Wilson L, Himes RH. Binding of vinblastine to stabilized microtubules. Mol Pharmacol 1989;36:366–70.
36. Panda D, Jordan MA, Chu KC, Wilson L. Differential effects of vinblastine on polymerization and dynamics at opposite microtubule ends. J Biol Chem 1996;271:29807–12.
37. Roach MC, Ludueña RF. Different effects of tubulin ligands on the intrachain cross-linking of β 1-tubulin. J Biol Chem 1984;259: 12063–71.
38. Cormier A, Marchand M, Ravelli RB, Knossow M, Gigant B. Structural insight into the inhibition of tubulin by *Vinca* domain peptide ligands. EMBO Rep 2008;9:1101–6.

Molecular Cancer Therapeutics

Maytansine and Cellular Metabolites of Antibody-Maytansinoid Conjugates Strongly Suppress Microtubule Dynamics by Binding to Microtubules

Manu Lopus, Emin Oroudjev, Leslie Wilson, et al.

Mol Cancer Ther 2010;9:2689-2699.